Greca, Luiz G.; Rafiee, Mahdi; Karakoç, Alp; Lehtonen, Janika; Mattos, Bruno D.; Tardy, Blaise L.; Rojas, Orlando J.

Guiding Bacterial Activity for Biofabrication of Complex Materials via Controlled Wetting of Superhydrophobic Surfaces

Published in:
ACS Nano

DOI:
10.1021/acsnano.0c03999

Published: 27/10/2020

Document Version
Peer-reviewed accepted author manuscript, also known as Final accepted manuscript or Post-print

Please cite the original version:
Greca, L. G., Rafiee, M., Karakoç, A., Lehtonen, J., Mattos, B. D., Tardy, B. L., & Rojas, O. J. (2020). Guiding Bacterial Activity for Biofabrication of Complex Materials via Controlled Wetting of Superhydrophobic Surfaces. *ACS Nano*, *14*(10), 12929-12937. https://doi.org/10.1021/acsnano.0c03999

Guiding Bacterial Activity for Biofabrication of Complex Materials *via* Controlled Wetting of Superhydrophobic Surfaces

Luiz G. Greca,[*,1] Mahdi Rafiee,[1] Alp Karakoç,[1,2] Janika Lehtonen,[1] Bruno D. Mattos,[1] Blaise L. Tardy,*[*,1] Orlando J. Rojas*[*,1,3]

[1] Department of Bioproducts and Biosystems, School of Chemical Engineering, Aalto University, P. O. Box 16300, FI-00076 Aalto, Finland

[2] Department of Communications and Networking, School of Electrical Engineering, Aalto University, P. O. Box 15500, FI-00076 Aalto, Finland

[3] Departments of Chemical and Biological Engineering, Chemistry and Wood Science, University of British Columbia, 2360 East Mall, Vancouver, BC V6T 1Z4, Canada.

E-mail: orlando.rojas@aalto.fi, blaise.tardy@aalto.fi, luiz.greca@aalto.fi

ABSTRACT

Superhydrophobic surfaces are promising for preventing fouling and the formation of biofilms, with important implications in the food chain, maritime transport, health sciences, among others. In this work, we exploit the interplay between wetting principles of superhydrophobic surfaces

and microbial fouling for advanced three-dimensional (3D) biofabrication of biofilms. We utilize hydrostatic and capillary pressures on superhydrophobic surfaces to finely control the air-water interface and the aerotaxis-driven biofabrication. Superhydrophobic 3D molds are produced by a simple surface modification that partially embeds hydrophobic particles in silicone rubber. Thereafter, the molds allow the templating of the air-water interface of the culture medium, where the aerobic nanocellulose-producing bacteria (*Komagataeibacter medellinensis*) are incubated. The biofabricated replicas are hollow and seamless nanofibrous objects with controlled morphology. Gradients of thickness, topographical feature size and fiber orientation on the biofilm are obtained by controlling wetting, incubation time and nutrient availability. Furthermore, we demonstrate that capillary length limitations are overcome by using pressurized closed molds, whereby a persistent air plastron allows the formation of 3D microstructures, regardless of their morphological complexity. We also demonstrate that interfacial biofabrication is maintained for at least 12 days without observable fouling of the mold surface. In summary, we achieve controlled biofouling of the air-water interface as imposed by the experimental framework under controlled wetting. The latter is central to both microorganism-based biofabrication and fouling, which are major factors connecting nanoscience, synthetic biology and microbiology.

Keywords: bacterial motility, capillary wetting, chemotaxis, living materials, nanofiber alignment, fouling, superhydrophobic surfaces

Understanding the interactions of bacteria at interfaces is crucial to multiple fields of science, with important societal, environmental and economic implications.[1] Associated with the controlled fouling of interfaces, two very important challenges arise; (i) developing long-lasting antifouling

surfaces, and (ii) achieving optimal control over 3D-biofabrication of advanced materials. While current discussions often consider these challenges independently, they may benefit from cross-disciplinary insights related to interfacial[2,3] and bulk-related[4] physico-chemical factors affecting bacterial behavior. Superhydrophobization of surfaces is among the most promising options to address challenge (i), namely, antifouling applications. The working mechanism in this approach is linked to the existence of an air layer (plastron) between water and a rough hydrophobic surface. In general, this air plastron is intended to inhibit surface attachment of bacteria or microorganisms.[5–7] Compared to typically wetting surfaces, superhydrophobic ones reduce adhesion by decreasing the solid-liquid interfacial area and associated attachment points.[6,7] The lifetime of an air plastron in a highly-fouling, bacterial environment, however, is not yet fully agreed upon.[8] For instance, immersed superhydrophobic surfaces can be very short-lived (*ca.* 2.5 h) due to gas dissolution (from the air plastron) in water.[8] In the animal kingdom, however, air plastrons can be retained for long periods (several months), for example, on the hairy surfaces of insects and spiders that utilize the plastron for breathing (plastron respiration).[9] It is therefore evident that better understanding of fouling events[2,10,11] and plastron dissolution[9] is needed, both of which are highly dependent on the physico-chemical characteristics of immersed surfaces. Insights may arise from recent work that introduced air plastrons to sustain a three-dimensional (3D) oxygen source for the interfacial, aerobic, biofabrication of nanocellulose-based biofilms.[12,13] In contrast with fully wetted surfaces, resulting biofilms replicate the 3D morphology of the template. Such 3D-biofabrication method offers the opportunity to further investigate the dynamics of biofouling events on superhydrophobic surfaces.

Regarding challenge (ii), *i.e.,* optimal control over biofabrication, bacteria and associated biofilms bear a promising future for the development of programable materials possessing

advanced properties.[14,15] For instance, the naturally optimized and highly crystalline extra-cellular matrix of nanocellulose-based biofilms (bacterial nanocellulose, BNC) has also been a prime choice for applications in biomedical engineering, with a particular focus on tissue templating.[16–20] However, limited progress has been achieved in this latter direction. Even though many biofabrication techniques have recently emerged,[16–24] full control over the complex physical characteristics (*e.g.*, shape, topography, stiffness), coupled with gradients of fundamental importance for biological functions in nature, has yet to be achieved. One of the more pressing matters is the limited knowledge on the correlation between physico-chemical characteristics of confined 3D-culture environments and biosynthetic factors driving bacterial behavior and biofilm formation.[4,25] Ultimately, understanding the way bacteria sense (chemotaxis) and navigate through their environment towards nutrient sources (optimal foraging theory) will greatly impact our capacity to control the structure and associated function of engineered biofilms.

Considering the challenges and opportunities orbiting in the areas of antifouling surfaces and advanced biofabrication, we herein develop an experimental framework to demonstrate how superhydrophobic 3D-molds can be used to control bacteria activity at interfaces. We explore the interplay between the physico-chemical characteristics of the confined medium, the associated superhydrophobic interfaces and the biosynthetic considerations driving bacterial behavior and biofilm formation (Figure 1). With the 3D biofabrication used herein, hydrostatic pressure simultaneously governs mold wetting and oxygen access to bacteria, both being of prime importance in biofilm formation. Therefore, by using such variables, we achieve gradients of topographical features, film thickness, and BNC fiber alignment. Furthermore, we demonstrate the persistence of the air plastron for at least 12 days in fouling conditions, which is in contrast with the short-life span of a completely immersed plastron.[8] In summary, the results presented provide

important guidelines leading to (i) long-lasting antifouling and, (ii) optimal control over the multi-scaled morphology and functions of living-materials.

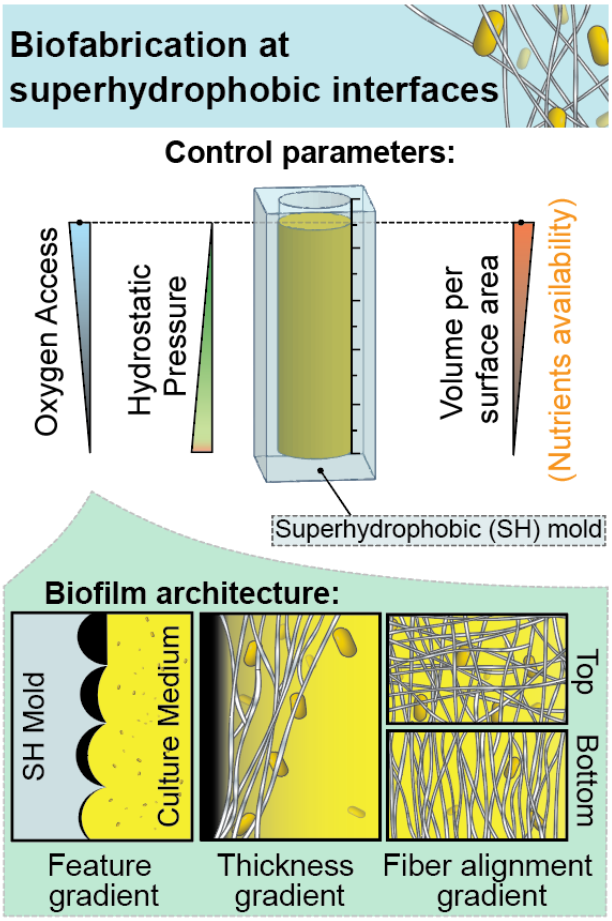

Figure 1. Schematic illustration of superhydrophobic 3D molds used to guide bacterial behavior and biofilm formation.

RESULTS AND DISCUSSION

Fabrication of Elastic Superhydrophobic Molds

In order to evaluate our proposed platform for controlling bacteria interactions at interfaces, room-temperature-vulcanizing (RTV) silicone rubber was used to produce molds that were superhydrophobized by simply spreading poly(tetrafluoroethylene) (PTFE) powder (*ca.* 35 μm average size) inside the cavity of the molds (Figure 2a and Video S1). This superhydrophobization

method resembles the PTFE particles-embedding technique we developed previously,[12] but with the advantage of being solvent-free. Significant adhesion between the silicone surface and the PTFE particles was achieved through a combination of interactions, including elastocapillary,[26] triboelectric[27] and van der Waals.[28] The particles were partially embedded onto the soft silicone surface (Figure 2b), onto which they remained adhered even after 30 min of water bath untrasonication (Figure 2c). As can be seen in Figure 2d, the combination of the low surface energy and roughness of the well-adhered PTFE particles resulted in water contact angles of 155 ± 6° on the coated surface, and 154 ± 6° after ultrasonication (Figure 2d), evidencing the good adhesion of the PTFE particles to the molds.

In contact with water, the superhydrophobized surface or, more specifically, the air plastron formed therein, became a source of oxygen for the aerobic, nanocellulose-producing microorganism (*Komagataeibacter medellinensis*) incubated in a modified Hestrin-Schramm (HS) culture medium. Such proposed approach resembles an inverted plastron breathing and is significantly different and faster compared to current methods for 3D-biofabrication involving the use of thin, oxygen-permeable silicone molds.[16,17] Furthermore, if compared to superhydrophobized 3D-printed molds,[12] the method herein described is expected to enable a broader range of biofabrication strategies and shape complexity, given the facile demolding enabled by the elasticity of the silicone.

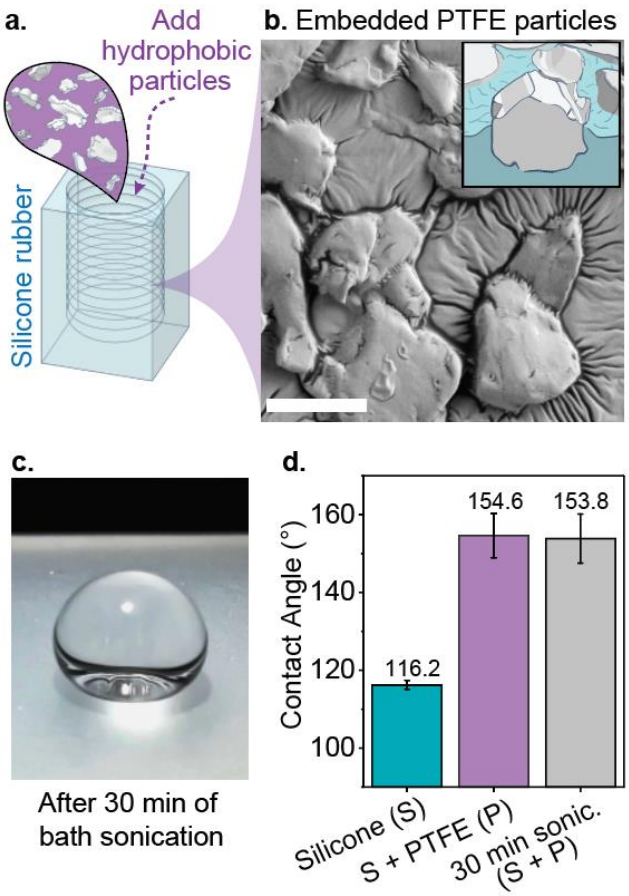

Figure 2. a) Schematic representation of the superhydrophobization method used for mold manufacturing. b) SEM image depicting the silicone rubber surface after the addition of the solvent-free hydrophobic powder (PTFE particles, 35 µm average size) and the resulting particle embedding (scale bar is 10 µm). c) Water droplet on the superhydrophobic surface after 30 min of continuous water bath ultrasonication, evidencing good adhesion of the PTFE particles to the silicone rubber. Internal reflections associated with the underlying plastron can be seen. d) Water contact angles of the pristine (uncoated) silicone rubber surface (S) and the PTFE-coated silicone (S+PTFE (P)) before and after 30 min ultrasonication.

Microbial Ecology Considerations to Guide 3D-Biofabrication

The effect of access to oxygen and nutrient availability over given incubation times were evaluated by incubating the nanocellulose-producing bacteria inside molds of varying depth (between *ca.* 6 and 12 cm). Upon formation of the BNC objects for 7 days, they were cut into sections with depth intervals of ~1 cm (Figure 3a1). The mass per unit surface area (or areal density, *D*) of each section was determined and related to the respective vertical position they were taken from. Considering the homogeneity of the material, *D* is herein assumed to be related to the thickness of the biofilm. For a 12 cm high BNC object, *D* decreased linearly with the distance measured from the top, with a 50% lower *D* at a depth of *ca.* 9 cm. Thereafter, *D* remained nearly constant at positions further down from the top surface, from 9 cm to 12 cm, see Figure 3a2. Evaluation of a smaller object (6 cm high) indicated the same trend and a similar decay rate of *D*. These results suggest a decrease in oxygen accessibility going down from the top of the object to its bottom. It can be reasonably proposed that this effect is related to the increasing hydrostatic pressure exerted by the (liquid) culture medium, which increasingly forces contact with the rough surface of the superhydrophobic mold (Figure 3a1).[29] Another consideration is related to the design of the mold with an exposed, open top section that facilitates oxygen renewal.

In an attempt to control the gradient of *D*, the previous observations were tested on cylindrical objects (5 mm radius) biofabricated with different incubation times, Figure 3b. A 7.7 cm^3 object (*ca.* 10 cm of height) produced by incubation during 4 days showed a steeper reduction in *D* than those produced during 12 days (slopes of −0.121 mg cm^{-3} and −0.006 mg cm^{-3}, respectively). Furthermore, the decrease in *D* was also more pronounced in an object produced in 4 days compared to samples previously produced in 7 days (Figure 3a2), which had a slope of *ca.* −0.04 mg cm^{-3}. The results point to a reduced cumulative gradient of oxygen access along the vertical coordinate when longer biofabrication times were used. This observation likely resulted from the

lower oxygen access across the thicker BNC biofilm formed at the top sections of the respective object. This is supported by the linear decrease in oxygen concentration with the increasing distance from the air-water interface, thus directly affecting bacterial activity.[30] Such effect counterbalances the higher oxygen access at the top sections occurring in early biofabrication periods.

In summary, our results show that hydrostatic pressure and incubation time control the gradients of thickness (proportional to *D*), which may consequently translate as gradients of mechanical properties that play a key role in different applications, including tissue engineering.[31] Furthermore, from a fouling perspective, the results indicate that the air plastron of the superhydrophobic surface remained unaffected for approximately 12 days under a highly fouling environment. From a generalized and practical standpoint, this implies that the optimal utilization of superhydrophobic surfaces may require that the air plastron is kept open to ambient air to avoid its depletion when subjected to prolonged contact with water.

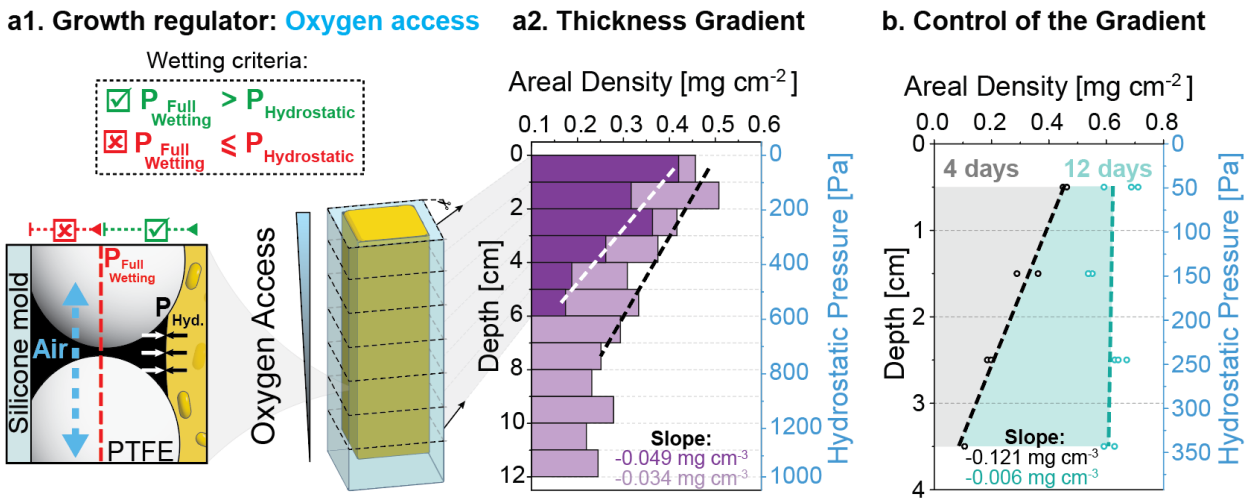

Figure 3. a1) Schematic illustration describing the experimental set up used for biofabrication and the relationship between the hydrostatic pressure ($P_{Hydrostatic}$) and full wetting capillary pressure ($P_{Full\ Wetting}$). Such relationship governs the existence of the air plastron, where $P_{Hydrostatic}$ must be

lower than $P_{Full\ Wetting}$. a2) Effect of the hydrostatic pressure on biofabricated objects of 6 and 12 cm of height. b) Effect of time on the biofabrication of cylindrical objects of 7.7 cm^3 (*ca.* 10 cm high). The thickness is herein assumed to be proportional to the areal density of the biofilm.

The effect of nutrient availability per unit surface area is illustrated in Figure 4a1,a2, where the *D* values from the top section of cylindrical objects of given volume (V)-to-surface area (SA) ratios ($V\ SA^{-1}$) were analyzed. $V\ SA^{-1}$ was controlled by varying the volume of culture medium added to the molds of exact same dimensions. The top section of the biofabricated objects was evaluated to draw comparisons at a similar oxygen access across objects of different height. Different incubation periods (4 and 12 days) were used to account for the time necessary for nutrient depletion, which curtails biofilm growth. As can be observed from Figure 4a2, the areal density increased approximately linearly with the $V\ SA^{-1}$ ratio of the objects. Such a trend, for biofilms grown for 12 days, indicates that larger volumes (larger $V\ SA^{-1}$) have access to larger amounts of nutrients per unit of surface area, allowing the production of thicker biofilms. No significant differences, however, could be seen for *D* at the top section for objects that were grown during 4 days.

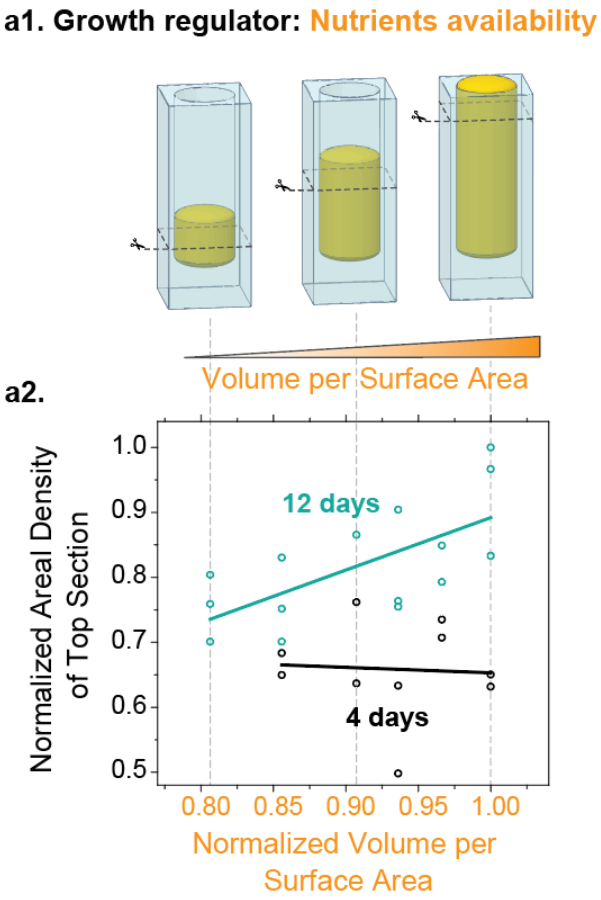

Figure 4. a1) Schematic illustration of the experimental setup used to evaluate the a2) effect of nutrient availability on the interfacial biofabrication, as regulated by different volume per surface area ratios and incubation time (4 and 12 days). The green and black lines are included as a guide to the eye.

Wetting and Fouling Considerations to Control 3D-Physical Gradients

We evaluated how the hydrostatic pressure and fouling affect the conformation of the air-water interface in relation to the surface features of the mold (fidelity of replication). For this purpose, we used silicone molds with horizontal micro-scaled features of three different sizes, which were superhydrophobized and later used for biofabrication. 3D-printed cylinders of different printing resolution were used as a master template for the negative, silicone molds having horizontal

grooves of 80, 160 and 320 μm of width. As proposed in the schematic illustration in Figure 5a1, after culture medium is added to the molds, the air-water interface gradually changes curvature as a result of increasing depth and hydrostatic pressure. The capillary pressure of the grooves is overcome at deeper sections of the mold and the culture medium partially wets the microscopic features. During biofabrication, these features are recorded (imprinted) in the biofilms analyzed after removal from the mold (Figure 5a2,a3). The replication fidelity for the sample featuring 320 μm grooves was further evaluated by measuring the height of the protrusion of the features replicated in the biofilms as a function of the depth (hydrostatic pressure) (Figure 5b).

When the biofabricated objects are compared for their feature height at the upper sections (less than 3 cm measured from the top), the fidelity of feature replication progressively reduced for the objects carrying grooves widths of 160 and 80 μm (from partial to no replication, respectively). Nearly no replication was observed at such small hydrostatic pressure and feature size. At increasing depths, the higher hydrostatic pressure made the air-water interface to gradually penetrate into the grooves (Figure 5a2,a3). A clear threshold to achieve maximum feature resolution was observed (Figure 5a2,b). For all molds, the hydrostatic pressure at such depth threshold was comparable to the capillary pressure at the grooves. Here, the Young-Laplace equation was used, taking into account the contact angle of the culture medium on the PTFE particle-coated flat silicone (151 ±4°) and considering the surface tension of the bacteria-containing culture medium (Figure S2 and S3). The slight difference between hydrostatic and capillary pressures required to reach maximum feature resolution, was likely caused by topographical effects, which might drive the bacteria towards the valleys of the grooves.[10,11] Such behavior could result in a reduction of the local surface tension caused by the bacteria acting as surface active particles (Figure S2), and by the localized production of surfactants.[32] However,

infiltration of capillary features of different geometries and surface characteristics under fouling environments, is a subject that needs further consideration. The objects containing 80 μm grooves were not as uniform as the ones containing larger features. This may be caused by the uneven distribution of the PTFE particles on the smaller grooves due to the size of the flake-like particles (few μm in thickness and *ca.* 10 to 75 μm in their principal plane) (Figure S1). Therefore, we suggest that the size of the hydrophobic particles needs to be considered when their dimensions approach those of the topographical features to be superhydrophobized. Nevertheless, the molds having grooves of 80 μm resulted in areas of high resolution at the lower sections, with the smallest features of the mold being fully replicated by the biofilm as valleys < 10 μm wide (Figure 5c1,c2). From a biofabrication perspective, increasing hydrostatic pressure, although potentially detrimental to the oxygen availability, can be used to regulate and enhance the fidelity of replication of small features. Furthermore, the results reveal the possibility of not only controlling gradients of thickness, but also of topographical features.

Importantly, as a result of the gradient of oxygen access, the BNC fibrils formed in the vicinity of the features were aligned in the vertical direction, parallel to the oxygen gradient (Figure 5c2). In fact, the alignment was observed to be more pronounced at the bottom section of the objects, with the topmost fibrils having mostly random orientation (Figure S4). Such gradient of alignment in the biofilm is observed to span across the length of the centimeter-long BNC objects. This observation is likely a result from aerotaxis, where aerobic bacteria sense different concentrations of oxygen in their environment and are therefore attracted to regions of optimal oxygen concentration.[30] This is an example of how optimal foraging theory can be used in materials science, where a controlled micro- and macro-environment gradient can be utilized to tailor

bacterial behavior and thus engineer biofilm production. All physical gradients presented herein are important for a wide range of applications,[33] especially in biomedicine.[31,34]

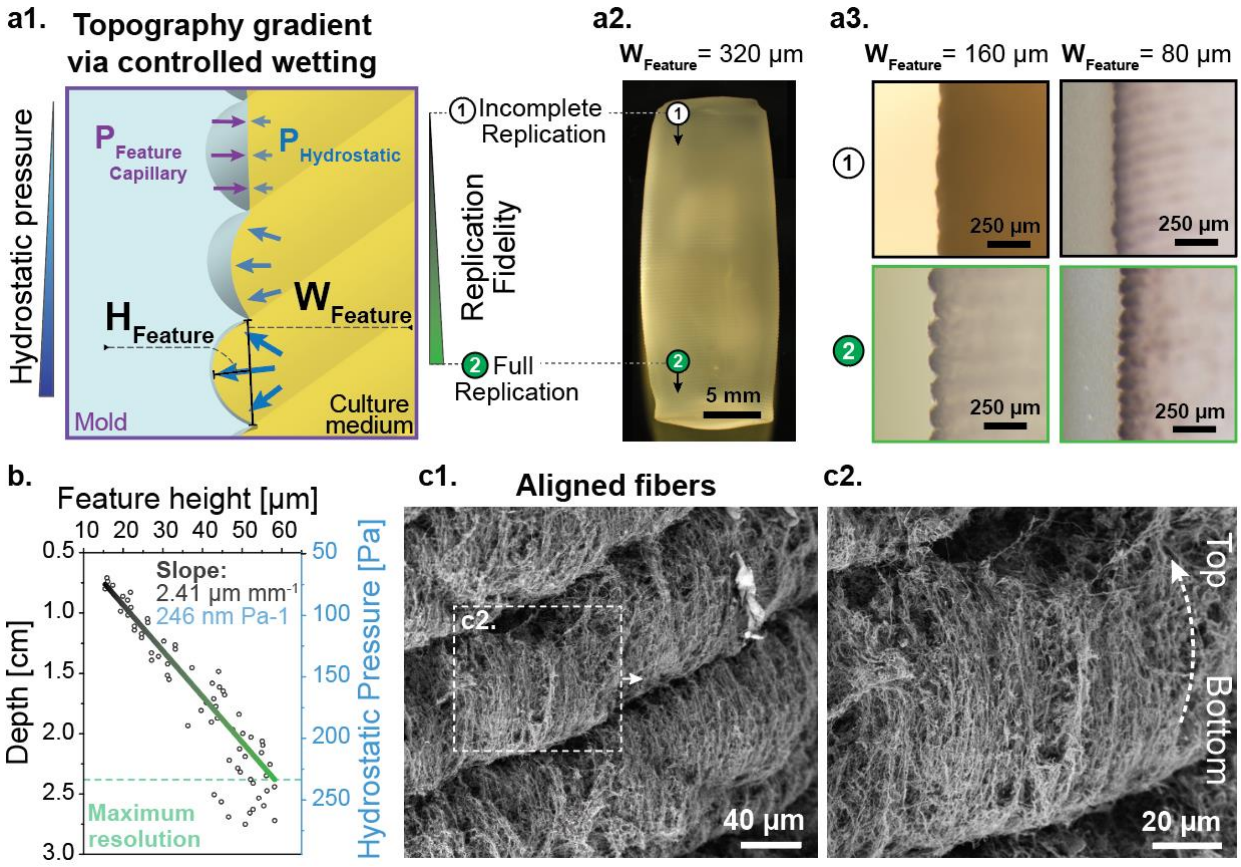

Figure 5. a1) Schematic representationof the fidelity of replication as a function of hydrostatic pressure. Optical microscopy from the biofabricated object with features width ($W_{Feature}$) of a2) 320 µm (oblate shape is due to partial collapse of the object evaluated herein during imaging), a3) 160 µm (left) and 80 µm (right). The gradient of feature height on the biofabricated object depicted in a2 can be seen in high resolution in Figure S5. b) Height of the feature as a function of depth and corresponding hydrostatic pressure for the sample having $W_{Feature}$ = 320 µm. c1) SEM of the lower, outside surface of a supercritically dried, hollow, nanocellulose cylinder with 80 µm

features. c2) Aligned nanocellulose fibers following the upward direction of the mold are highlighted.

Increased Replication Fidelity in Closed Molds

We next expand on the biofabrication of 3D complex morphologies by exploiting the relationship between wetting, hydrostatic pressure and fidelity of object replication. The biofabrication of intricate features below the capillary length, a dimension at which features cannot be well replicated due to high capillary pressure, was evaluated using fractal vascular networks (Figure 6a). In such a context, the hydrostatic pressure required to overcome the capillary pressure of progressively smaller tubes ($P_{Feature\ Capillary}$) continuously increases to the point that the culture medium no longer fills all the features of the mold, *e.g.,* under hydrostatic pressure alone. This presents one of the most significant challenges for such templated biofabrication (Figure S6) but also offers a significant benefit since such architectures form in a seamless fashion, representing a necessary step in scaffolding. Such scaffolds are highly sought after for high surface area organs possessing fractal structures, such as kidneys or lungs.

To overcome such challenge, closed molds in which the culture medium could be introduced with a syringe (Figure 6b) were designed to overcome the high hydrostatic pressure required for the complete replication of the smallest branches of a fractal mold cavity (Figure S7). A cut continuously connected the surface and the cavity of the mold, following all branches (Figures 6b and S7,8). Such a cut was used as a micro-scaled inlet to avoid the dissolution of the air plastron, with excess layers of PTFE particles being used to keep the micro-separation between the faces of the cut. To remove the BNC object, the mold was carefully bent upwards, adding tensile stress to the cut surface of the mold. Such stress forced the cut open and allowed the careful release of the BNC object (Figure S8).

As can be seen in Figure 6c,d, branches with a minimum radius of 0.8 mm were obtained. While the large branches are well replicated, the smaller ones are not always resolved, possibly as a result of the manual injection where pressure is not fully controlled. Nevertheless, the integrity of the object was preserved. In summary, it is suggested that proper replication fidelity can be achieved by using different strategies to increase the hydrostatic pressure inside the mold. Such strategies include designing the smallest features at the bottom sections of the mold, using a large reservoir of culture medium on top of the main part of the mold, or using a device such as a syringe pump to control the volume injected to the system. Despite the recent advances in 3D printing of bacterial hydrogels, with excellent control over topology and 3D-interconectivity, such technique suffers from a limited choice of nozzle sizes and ink rheology, thus hampering high resolution (*e.g.* < 500 μm).[23] In superhydrophobic molding, on the other hand, the manipulation of the air-water interface using hydrostatic pressure allows control of topographical features down to the nanometer scale (*ca.* 250 nm Pa^{-1}, Figure 4b). Furthermore, to the best of our knowledge, such an interfacial control has not been achieved by other biofabrication techniques, and facilitates the design of biofilms with a high degree of control over their physical gradients (*i.e.* topography, biofilm thickness and fiber alignment).

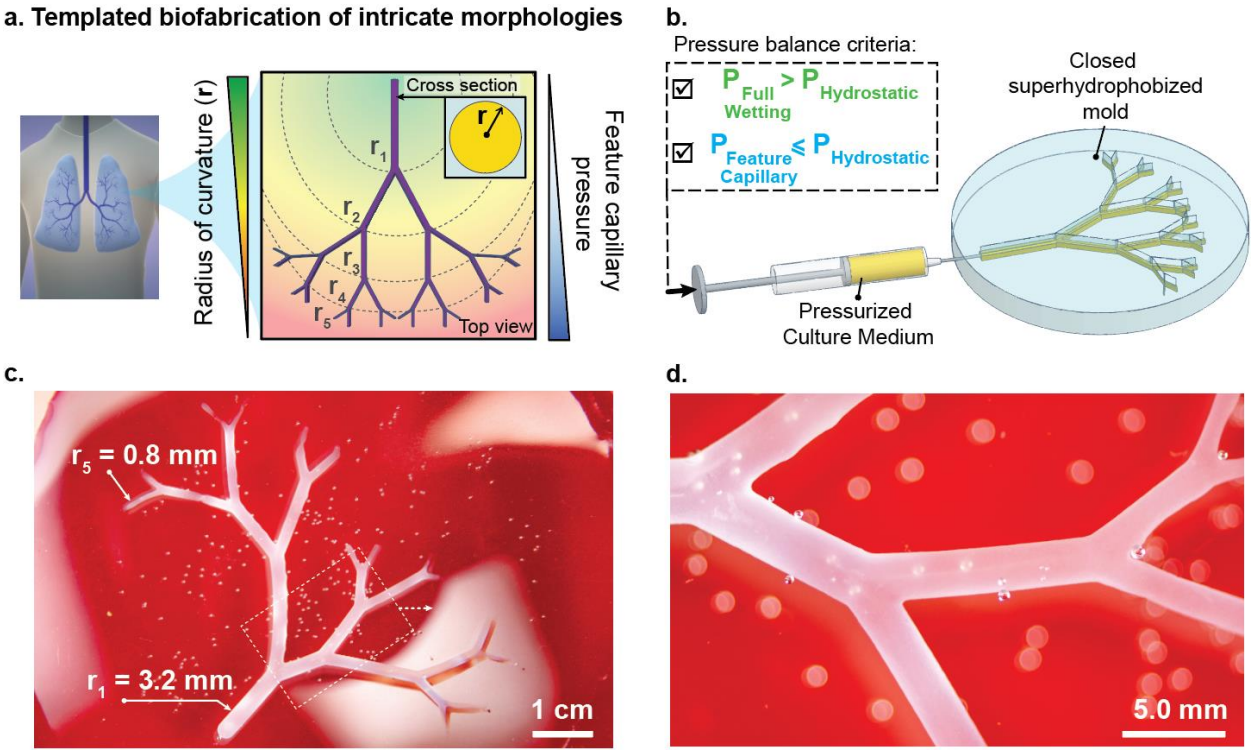

Figure 6. a) Schematic illustration showing the challenges associated with the biofabrication of complex biological architectures with the smallest features having radius of curvature below the capillary length (*ca.* 2.7 mm). b) Strategy used to overcome the high capillary pressure associated with the small features of the mold. c) and d) Biofabricated replica of fractal vascular constructs possessing features bellow the capillary length, produced by the strategy depicted in b).

CONCLUSIONS

We incubated cellulose-producing microorganisms (*Komagataeibacter medellinensis*) in 3D superhydrophobic molds and achieved fine control over biofilm formation by manipulating hydrostatic pressure, wetting and nutrient availability. Importantly, no genetic engineering methods were used but simple and affordable control of the physico-chemical characteristics of the environment to induce desired bacterial behavior.

Our results show the possibility of producing biofilms with a gradient of orientation of BNC fibrils, *i.e.*, from mostly random orientation at the topmost sections of the object, to vertically oriented at the bottommost sections. Such gradient scales with oxygen availability (proportional to biofabrication depth), hinting to the utilization of controlled wetting of superhydrophobic surfaces and optimal foraging theory for controlling material biofabrication. While fibril alignment along 1D and simple 2D BNC materials may be achieved by other techniques, currently, templating using superhydrophobic molds is the only mean to produce aligned fibrils in 3D-BNC objects. Furthermore, gradients of thickness and feature size were realized by controlling the hydrostatic pressure and biofabrication time. Importantly, by taking these control factors into account during the mold design, the gradients may be tuned and reproduced in a nearly limitless range of possible 3D shapes achievable by molding. Such physical gradients may play an important role in practical applications where the rapid optimization of physical properties of biofilms is required (combinatorial material science). When considering the outstanding biocompatibility of BNC, biomedical sciences may also benefit. For instance, fibril alignment, apparent stiffness and topography are variables that are known to guide cell growth and differentiation.

Moreover, long-lasting (at least 12 days) superhydrophobic surfaces under highly fouling environments were effectively achieved by ensuring plastron access to ambient air. This strategy was effective even when using partially closed molds, where high hydrostatic pressure was used for improving feature replication (resolution). These results are expected to further motivate investigations on design parameters to protect air plastrons from dissolution when using superhydrophobic surfaces under fouling environments.

Despite their interrelations, bacterial motility, biofouling phenomena and material biofabrication have been mostly investigated in isolation. Understanding and, specially, controlling bacteria

interactions at interfaces has therefore been challenging. We expect our interdisciplinary approach to shed light to the matter and foster future research connecting such fields with far reaching implications to antifouling, biomedicine, material science, bioengineering, microbiology and synthetic biology.

METHODS

Manufacturing of the silicone molds

The silicone molds used for biofabrication were produced according to the desired shape of the biofilm-based object. In short, two different mold fabrication methods were used, *i.e.*, a) 3D-printed templates (Figure S8) and, b) silicone tubes.

a) 3D-printed templates - Computer-aided design and 3D-printing using a Ultimaker 3 Extended were used to prepare a master for (negative) silicone molds. The 3D-printed masters, produced with polylactic acid (PLA), were placed in containers that were subsequently filled with silicone rubber. The rubber was a Pt-cured, bicomponent room-temperature-vulcanizing silicone, under the brand name Zhermack ZA13 Mould WT45. This silicone rubber has a hardness of *ca.* 13 shA and a strain at break of *ca.* 450 %. From our experience, silicone rubbers with similar mechanical characteristics, but from different brands and catalyst types (tin-cured, for example), behave similarly and are not a limitation for the superhydrophobization or biofabrication processes. Prior to the casting of the silicone, air bubbles were removed using a vacuum oven (50 mbar) at room temperature. After casting, the silicone was ambient-cured for at least 24 h. The 3D-printed masters were easily removed from the open molds by simple pulling action. When a closed mold was used, a cut was made with a razor blade for connecting the surface of the mold and the cavity generated by the 3D-printed master (Figures S7,8). Such a cut was done in such a way that the mold remained

in one single piece with a self-closing cut, which allowed the removal of the template (and later the equivalent BNC object) by simple bending (Figure S8).

Three different sets of templates were prepared: cuboids (cross section = 2 x 2 cm and height = 6 and 12 cm), cylinders (r = 5 cm and height = 3 and 12 cm) and fractal, branched shapes ("trees"). The cylinders were printed vertically using different printing resolutions, *i.e.*, 80, 160 and 320 μm. As the fused filament fabrication method used herein happens on a layered fashion, the resolution accounted for the height of the printed layer, and consequently generated what we describe as the characteristic "groove width" of the silicone mold. The molds for cuboids and cylinders remained with an open top face, as schematically shown in Figures 1, 2 and 3. The fractal vascular network was produced based on an algorithm for the modeling of a fractal tree, provided by the Rosetta code [https://rosettacode.org/wiki/Fractal_tree]. In this algorithm, a trunk was drawn and at the end of the trunk, two branches were formed. The angle between the branches was defined randomly in a selected domain between π/8 and π/2 rad. This process was repeated till the end of each branch reached a given distance from the trunk or till a given level of branching. A penalty condition was implemented, by which the models with intersecting branches were eliminated, and a fractal tree satisfying the condition criteria was randomly selected. In this case, the 3D-printed master was produced using an SLS 3D printer, resulting in an object with a smooth surface finishing. Such fractal vascular network was used for producing an open half-mold as well as a closed mold.

For contact angle measurements, flat silicone rubber sheets were fabricated.

b) Silicone rubber tubes - In the second method used for the fabrication of the molds, translucent silicone rubber tubes (inner diameter of 10 mm) were cut at lengths varying from 3 to 14 cm and were subsequently closed at one end by using the Zhermack ZA13 Mould WT45 silicone rubber.

Importantly, the silicone tubes were not reinforced and had similar mechanical properties to those of the silicone rubber used in method a). Differently from the 3D-printed objects, these tubes had smooth internal surfaces and were used for assessing the depletion of nutrients in objects of different V SA^{-1}, and for assessing the effect of biofabrication time on the thickness gradient.

Superhydrophobization

The inner walls of the prepared molds, as well as of the flat silicone surfaces, were hydrophobized using polytetrafluoroethylene (PTFE) powder with a mean particle size of 35 μm (Video S1). Excess powder was introduced inside of the cavity of the silicone molds, which were later closed and manually shaken for *ca.* 0.5 - 1 min. As the excess powder was removed (also using water), the PTFE particles were observed to form a well adhered layer on the surface of the silicone.

Preparation of the culture medium

The biofabrication was carried during 4, 7 and 12 days at 28 °C. *Komagataeibacter medellinensis* was incubated in a modified Hestrin-Schramm (HS) medium (20 g L^{-1} glucose, 5 g L^{-1} peptone, 5 g L^{-1} yeast extract and 2.5 g L^{-1} Na_2HPO_4). The components were dissolved in Milli-Q water and the pH was adjusted to 4.5 with citric acid. Such pH is near the optimal range for the *K. medellinensis* strain and is beneficial to restrict the growth of some common contaminants.[35] Nevertheless, the culture media were heated at 100 °C for at least 15 min and allowed to cool-down to room temperature prior to the inoculation of the bacteria.

Gravimetric analysis

The biofabricated objects were frozen at -20 °C while still inside of the molds. Then, the top side (cap) of each biofabricated object was removed using a razor blade. Pieces of 1 cm in height, corresponding to the biofilm produced at depth intervals of 1 cm, were subsequently cut and put

in DI water. The entire biofabricated objects were still frozen during the whole cutting procedure. Each piece was immediately washed to remove the culture medium and the remaining PTFE attached to the BC. The use of some ethanol in the washing cycles was observed to be beneficial for removing the PTFE. Between the washing cycles, the samples were stored separately at 4 °C. After washing, the pieces were carefully positioned on a non-sticking and flexible surface, dried and kept at 40 °C prior to weighing each piece. The distance between consecutive cuts, representing the height of each piece, was measured in at least three different positions. With such values, the area and the areal density of each piece was calculated.

Contact angle and surface tension measurements

Contact angle (CA) and surface tension measurements were carried using a CAM 200 optical contact angle goniometer (KSV instruments). The CA measurements were carried out using 6 µL of MilliQ water. The results represent the average and standard deviation from at least 4 measurements at different positions of a flat silicone rubber surface and a PTFE-particles coated silicone rubber surface. A durability test was performed by continuously ultrasonicating the coated surface in DI water during 30 min (Bandelin Sonorex Digitec), after which the contact angles were remeasured.. Surface tension measurements were performed by using the pendant drop method. The optimal volume of the droplet was estimated to be *ca.* 4.5 - 5.5 µL based on the Worthington number,[36] which takes into account the maximum pendant drop volume that a needle of 0.3 mm of nominal diameter can sustain (*ca.* 7.1 µL for water). The volume of the droplet was kept at *ca.* 5 µL.

Hydrostatic and capillary pressure

The capillary pressure was calculated as:

$$P_{Cap} = -\frac{2*\gamma*\cos\theta}{w}$$

where γ is the surface tension, θ is the measured culture medium contact angle of a superhydrophobized (using PTFE powder, 35 μm) silicone sheet (flat) and w is the width of the feature. By using optical microscopy, the depth at which the features achieved maximum resolution was estimated. Such depths were used to calculate their corresponding hydrostatic pressure.

Optical microscopy

The cross sections of the silicone molds with templated topography and the biofabricated objects were imaged by using an Olympus SZX10 optical microscope with a DP74 camera. The images from the biofilms were taken by placing the biofabricated objects on a Petri dish with DI water. When two or more images were needed to represent the whole sample, they were stitched by using the Adobe Photoshop CC 2018 software. The replicated height of the features was measured using the ImageJ 2.0.0-rc56/1.51h software. In short, an image of an object of *ca.* 30 mm height and 320 μm feature width was binarized by using the Otsu automatic thresholding method. Then, the height of the features was manually measured and plotted against the corresponding depth, *i.e.*, the distance relative to the top surface of the biofabricated object.

Scanning Electron Microscopy (SEM)

Two dimensional sheets were prepared from biofabricated cylindrical objects. In short, a sharp blade was used to remove the top and the bottom sections of the cylindrical biofilm and to subsequently cut the biofilm into smaller sections (*ca.* 3 cm). The resulting tube-shaped pieces were opened through a lateral cut parallel to the vertical axis of the biofilm. The resulting 2D samples were gradually solvent-exchanged to acetone and super-critically dried. The dried biofilms were placed on SEM stubs using carbon tape and coated with 5 nm of Au-Pd. Imaging

was performed using a field emission scanning electron microscope (FE-SEM, Zeiss SigmaVP, Germany) operating at 1.3 kV and a working distance of *ca.* 6 mm.

ASSOCIATED CONTENT

Table of Contents

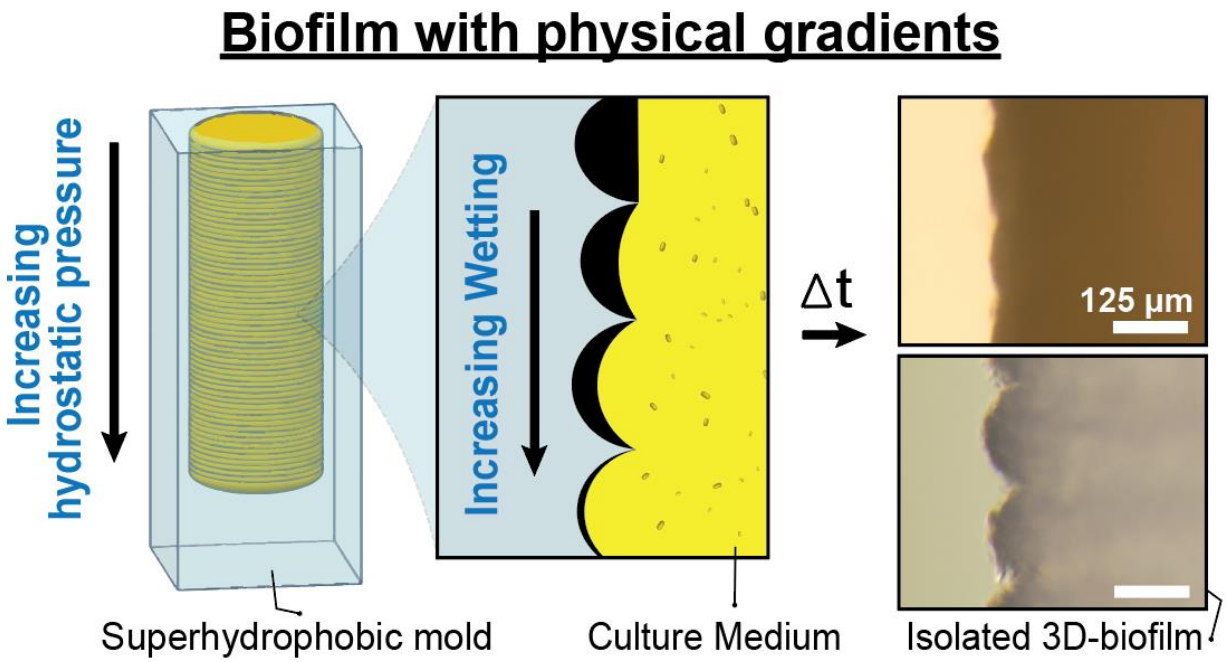

Supporting Information

The following files are available online free of charge at http://pubs.acs.org:

- Supporting figures: SEM, surface tension measurement, capillary and hydrostatic pressure comparison, optical microscopies, scheme depicting the mold manufacturing. (PDF).

- Video S1: Superhydrophobization *via* embedding of hydrophobic particles onto silicone rubber.

The authors declare no competing financial interest.

AUTHOR INFORMATION

Corresponding Authors

* **Prof. Orlando Rojas** - University of British Columbia, Departments of Chemical and Biological Engineering 2360 East Mall, Vancouver, BC V6T 1Z4, Canada. Aalto University, Department of Bioproducts and Biosystems, School of Chemical Engineering, P. O. Box 16300, FI-00076 Aalto, Finland. Tel: +358 50 512 4227, Email: orlando.rojas@aalto.fi

* **Dr. Blaise Tardy** - Department of Bioproducts and Biosystems, School of Chemical Engineering, Aalto University, P. O. Box 16300, FI-00076 Aalto, Finland. Tel: +358 50 59 79156, Email: blaise.tardy@aalto.fi

* **Luiz G. Greca** - Department of Bioproducts and Biosystems, School of Chemical Engineering, Aalto University, P. O. Box 16300, FI-00076 Aalto, Finland. Tel: +358 50 3841761, Email: luiz.greca@aalto.fi

ACKNOWLEDGMENT

We acknowledge support by the European Research Council under the European Union's Horizon 2020 research and innovation program (ERC Advanced Grant Agreement No. 788489, "BioElCell"). The Academy of Finland's Flagship Programme under Projects No. 318890 and 318891 (Competence Center for Materials Bioeconomy, FinnCERES) is also gratefully acknowledged. O.J.R. is thankful to the Canada Excellence Research Chair initiative and the Canada Foundation for Innovation (CFI). L.G.G. also acknowledges funding by the Aalto University School of Chemical Engineering doctoral programme. We appreciate the provision of

facilities and technical support by Aalto University at OtaNano – Nanomicroscopy Center (Aalto-NMC). Finally, we are indebted to Valeria Azovskaya of the Aalto's Materials Platform for the photos used in Figures 6c,d.

REFERENCES

(1) Erramilli, S.; Genzer, J. Influence of Surface Topography Attributes on Settlement and Adhesion of Natural and Synthetic Species. *Soft Matter* **2019**, *15*, 4045–4067.

(2) Jahed, Z.; Shahsavan, H.; Verma, M. S.; Rogowski, J. L.; Seo, B. B.; Zhao, B.; Tsui, T. Y.; Gu, F. X.; Mofrad, M. R. K. Bacterial Networks on Hydrophobic Micropillars. *ACS Nano* **2017**, *11*, 675–683.

(3) Oliveira, N. M.; Foster, K. R.; Durham, W. M. Single-Cell Twitching Chemotaxis in Developing Biofilms. *Proc. Natl. Acad. Sci.* **2016**, *113*, 6532–6537.

(4) Stocker, R. Marine Microbes See a Sea of Gradients. *Science* **2012**, *338*, 628–633.

(5) Genzer, J.; Efimenko, K. Recent Developments in Superhydrophobic Surfaces and Their Relevance to Marine Fouling: A Review. *Biofouling* **2006**, *22*, 339–360.

(6) Zhang, H.; Lamb, R.; Lewis, J. Engineering Nanoscale Roughness on Hydrophobic Surface - Preliminary Assessment of Fouling Behaviour. *Sci. Technol. Adv. Mater.* **2005**, *6*, 236–239.

(7) Scardino, A. J.; Harvey, E.; De Nys, R. Testing Attachment Point Theory: Diatom Attachment on Microtextured Polyimide Biomimics. *Biofouling* **2006**, *22*, 55–60.

(8) Hwang, G. B.; Page, K.; Patir, A.; Nair, S. P.; Allan, E.; Parkin, I. P. The Anti-Biofouling

Properties of Superhydrophobic Surfaces Are Short-Lived. *ACS Nano* **2018**, *12*, 6050–6058.

(9) Flynn, M. R.; Bush, J. W. M. Underwater Breathing: The Mechanics of Plastron Respiration. *J. Fluid Mech.* **2008**, *608*, 275–296.

(10) Efimenko, K.; Finlay, J.; Callow, M. E.; Callow, J. A.; Genzer, J. Development and Testing of Hierarchically Wrinkled Coatings for Marine Antifouling. *ACS Appl. Mater. Interfaces* **2009**, *1*, 1031–1040.

(11) Hou, S.; Gu, H.; Smith, C.; Ren, D. Microtopographic Patterns Affect *Escherichia coli* Biofilm Formation on Poly(Dimethylsiloxane) Surfaces. *Langmuir* **2011**, *27*, 2686–2691.

(12) Greca, L. G.; Lehtonen, J.; Tardy, B. L.; Guo, J.; Rojas, O. J. Biofabrication of Multifunctional Nanocellulosic 3D Structures: A Facile and Customizable Route. *Mater. Horiz.* **2018**, *5*, 408–415.

(13) Laromaine, A.; Tronser, T.; Pini, I.; Parets, S.; Levkin, P. A.; Roig, A. Free-Standing Three-Dimensional Hollow Bacterial Cellulose Structures with Controlled Geometry: *Via* Patterned Superhydrophobic-Hydrophilic Surfaces. *Soft Matter* **2018**, *14*, 3955–3962.

(14) Nguyen, P. Q.; Botyanszki, Z.; Tay, P. K. R.; Joshi, N. S. Programmable Biofilm-Based Materials from Engineered Curli Nanofibres. *Nat. Commun.* **2014**, *5*, 4945.

(15) Nguyen, P. Q.; Courchesne, N. M. D.; Duraj-Thatte, A.; Praveschotinunt, P.; Joshi, N. S. Engineered Living Materials: Prospects and Challenges for Using Biological Systems to Direct the Assembly of Smart Materials. *Adv. Mater.* **2018**, *30*, 1704847.

(16) Bodin, A.; Bäckdahl, H.; Fink, H.; Gustafsson, L.; Risberg, B.; Gatenholm, P. Influence of

Cultivation Conditions on Mechanical and Morphological Properties of Bacterial Cellulose Tubes. *Biotechnol. Bioeng.* **2007**, *97*, 425–434.

(17) Orelma, H.; Morales, L. O.; Johansson, L.-S.; Hoeger, I. C.; Filpponen, I.; Castro, C.; Rojas, O. J.; Laine, J. Affibody Conjugation onto Bacterial Cellulose Tubes and Bioseparation of Human Serum Albumin. *RSC Adv.* **2014**, *4*, 51440–51450.

(18) Klemm, D.; Schumann, D.; Udhardt, U.; Marsch, S. Bacterial Synthesized Cellulose - Artificial Blood Vessels for Microsurgery. *Prog. Polym. Sci.* **2001**, *26*, 1561–1603.

(19) Bottan, S.; Robotti, F.; Jayathissa, P.; Hegglin, A.; Bahamonde, N.; Heredia-Guerrero, J. A.; Bayer, I. S.; Scarpellini, A.; Merker, H.; Lindenblatt, N.; Poulikakos, D.; Ferrari, A. Surface-Structured Bacterial Cellulose with Guided Assembly-Based Biolithography (GAB). *ACS Nano* **2015**, *9*, 206–219.

(20) Geisel, N.; Clasohm, J.; Shi, X.; Lamboni, L.; Yang, J.; Mattern, K.; Yang, G.; Schäfer, K. H.; Saumer, M. Microstructured Multilevel Bacterial Cellulose Allows the Guided Growth of Neural Stem Cells. *Small* **2016**, *12*, 5407–5413.

(21) Rühs, P. A.; Storz, F.; López Gómez, Y. A.; Haug, M.; Fischer, P. 3D Bacterial Cellulose Biofilms Formed by Foam Templating. *npj Biofilms Microbiomes* **2018**, *4*, 21.

(22) Schaffner, M.; Rühs, P. A.; Coulter, F.; Kilcher, S.; Studart, A. R. 3D Printing of Bacteria into Functional Complex Materials. *Sci. Adv.* **2017**, *3*, eaao6804.

(23) Shin, S.; Kwak, H.; Shin, D.; Hyun, J. Solid Matrix-Assisted Printing for Three-Dimensional Structuring of a Viscoelastic Medium Surface. *Nat. Commun.* **2019**, *10*, 4650.

(24) Rühs, P. A.; Malollari, K. G.; Binelli, M. R.; Crockett, R.; Balkenende, D. W. R.; Studart,

A. R.; Messersmith, P. B. Conformal Bacterial Cellulose Coatings as Lubricious Surfaces. *ACS Nano* **2020**, *14*, 3885-3895.

(25) Wessel, A. K.; Hmelo, L.; Parsek, M. R.; Whiteley, M. Going Local: Technologies for Exploring Bacterial Microenvironments. *Nat. Rev. Microbiol.* **2013**, *11*, 337–348.

(26) Style, R. W.; Hyland, C.; Boltyanskiy, R.; Wettlaufer, J. S.; Dufresne, E. R. Surface Tension and Contact with Soft Elastic Solids. *Nat. Commun.* **2013**, *4*, 2728.

(27) Bayer, I. S.; Brandi, F.; Cingolani, R.; Athanassiou, A. Modification of Wetting Properties of Laser-Textured Surfaces by Depositing Triboelectrically Charged Teflon Particles. *Colloid Polym. Sci.* **2013**, *291*, 367–373.

(28) Krupp, H.; Sperling, G. Theory of Adhesion of Small Particles. *J. Appl. Phys.* **1966**, *37*, 4176–4180.

(29) Emami, B.; Hemeda, A. A.; Amrei, M. M.; Luzar, A.; Gad-el-Hak, M.; Vahedi Tafreshi, H. Predicting Longevity of Submerged Superhydrophobic Surfaces with Parallel Grooves. *Phys. Fluids* **2013**, *25*, 062108.

(30) Zhulin, I. B.; Bespalov, V. A.; Johnson, M. S.; Taylor, B. L. Oxygen Taxis and Proton Motive Force in Azospirillum Brasilense. *J. Bacteriol.* **1996**, *178*, 5199–5204.

(31) Cai, P.; Layani, M.; Leow, W. R.; Amini, S.; Liu, Z.; Qi, D.; Hu, B.; Wu, Y. L.; Miserez, A.; Magdassi, S.; Chen, X. Bio-Inspired Mechanotactic Hybrids for Orchestrating Traction-Mediated Epithelial Migration. *Adv. Mater.* **2016**, *28*, 3102–3110.

(32) Rhodeland, B.; Hoeger, K.; Ursell, T. Rapid and Directed Group Motility in *B. subtilis* Does Not Rely on Individual Motility or Chemotaxis. *bioRxiv* **2020**, 719245.

https://doi.org/10.1101/719245 (accessed 09 02, 2020).

(33) Genzer, J.; Bhat, R. R. Surface-Bound Soft Matter Gradients. *Langmuir* **2008**, *24*, 2294–2317.

(34) Park, J. S.; Kim, D. H.; Kim, H. N.; Wang, C. J.; Kwak, M. K.; Hur, E.; Suh, K. Y.; An, S. S.; Levchenko, A. Directed Migration of Cancer Cells Guided by the Graded Texture of the Underlying Matrix. *Nat. Mater.* **2016**, *15*, 792–801.

(35) Castro, C.; Zuluaga, R.; Álvarez, C.; Putaux, J. L.; Caro, G.; Rojas, O. J.; Mondragon, I.; Gañán, P. Bacterial Cellulose Produced by a New Acid-Resistant Strain of Gluconacetobacter Genus. *Carbohydr. Polym.* **2012**, *89*, 1033–1037.

(36) Berry, J. D.; Neeson, M. J.; Dagastine, R. R.; Chan, D. Y. C.; Tabor, R. F. Measurement of Surface and Interfacial Tension Using Pendant Drop Tensiometry. *J. Colloid Interface Sci.* **2015**, *454*, 226–237.